Lawrence Berkeley National Laboratory
Lawrence Berkeley National Laboratory

Title
Performance of actinic EUVL mask imaging using a zoneplate microscope

Permalink
https://escholarship.org/uc/item/2889p68b

Authors
Goldberg, Kenneth A.
Naulleau, Patrick P.
Barty, Anton
et al.

Publication Date
2007-08-20

eScholarship.org Powered by the California Digital Library
University of California

Performance of actinic EUVL mask imaging using a zoneplate microscope

Kenneth A. Goldberg[1], Patrick P. Naulleau[1], Anton Barty[2], Senajith B. Rekawa[1], Charles D. Kemp[1], Robert F. Gunion[1], Farhad Salmassi[1], Eric M. Gullikson[1], Erik H. Anderson[1], Hak-Seung Han[3]

[1]Center for X-Ray Optics, Lawrence Berkeley National Laboratory, Berkeley, CA 94720, USA
[2]Lawrence Livermore National Laboratory, PO Box 808, Livermore, CA 94550, USA
[3]SEMATECH, 255 Fuller Road, Suite 309, Albany, NY 12203, USA

ABSTRACT

The SEMATECH Berkeley Actinic Inspection Tool (AIT) is a dual-mode, scanning and imaging extreme-ultraviolet (EUV) microscope designed for pre-commercial EUV mask research. Dramatic improvements in image quality have been made by the replacement of several critical optical elements, and the introduction of scanning illumination to improve uniformity and contrast. We report high quality actinic EUV mask imaging with resolutions as low as 100-nm half-pitch, (20-nm, 5× wafer equivalent size), and an assessment of the imaging performance based on several metrics. Modulation transfer function (MTF) measurements show high contrast imaging for features sizes close to the diffraction-limit. An investigation of the illumination coherence shows that AIT imaging is much more coherent than previously anticipated, with σ below 0.2. Flare measurements with several line-widths show a flare contribution on the order of 2–3% relative intensity in dark regions above the 1.3% absorber reflectivity on the test mask used for these experiments. Astigmatism coupled with focal plane tilt are the dominant aberrations we have observed. The AIT routinely records 250–350 high-quality images in numerous through-focus series per 8-hour shift. Typical exposure times range from 0.5 seconds during alignment, to approximately 20 seconds for high-resolution images.

Keywords: extreme ultraviolet lithography, EUV, mask inspection, zoneplate, imaging, actinic inspection.

1. INTRODUCTION

In EUV lithography, the surface of a patterned mask is a complex optical system constructed from many different materials: a low-thermal-expansion glass substrate, the reflective multilayer coating, a buffer layer to protect the multilayer during processing, and a patterned absorber layer. The acute sensitivity to the wavelength-dependent material properties and resonant-reflective multilayer mirror structure makes inspection with EUV light a necessary step in the technology development process. Whether EUV "actinic" inspection will be required in production is a subject of open debate; yet in this pre-commercial period, it is clear that the early availability of high-quality aerial image measurements from patterned masks is proving detailed feedback for reticle development, defect sensitivity evaluation, input to modeling, and answers to other important research questions. Aerial image inspection is complementary to lithographic printing; it provides continuous image intensity data at high resolution without the constraints of photo-resist printing.

The SEMATECH Berkeley Actinic Inspection Tool (AIT) is a unique dual-mode EUV microscope that operates in two distinct modes[1,2,3]. In *scanning mode* the tool measures the reflectivity and scattering properties of EUV masks with spatial resolution from 1–5 µm, and 0.1–0.2% sensitivity. In *imaging mode*, the tool operates as a high-resolution EUV zoneplate microscope, measuring the reflected intensity directly, *at-wavelength*, with spatial resolution designed to emulate a 0.25 NA stepper. The AIT has recently undergone significant upgrades and improvements that have enabled high-quality imaging. The performance characteristics of imaging mode is the subject of this report.

Following a description of the system configuration and operating parameters, we present a calculation of the modulation transfer function (MTF) based on thousands of individual through-focus-series images. We have imaged similar bright-field and dark-field "elbow" resolution test patterns, lines for line-edge and line-width roughness assessment, and dark crosses in a bright field for flare testing. Furthermore, the observed focal plane shape and astigmatism magnitude will be addressed.

2. SYSTEM DESIGN

The AIT operates on a bending magnet beamline at the Advanced Light Source, Lawrence Berkeley National Laboratory. The beamline provides stable, EUV illumination with a tunable bandwidth and wavelength, centered at 13.4-nm. The configuration of the AIT is shown in Fig. 1. The mask position under the stationary beam is controlled by a rotation and translation stage, $x\theta z$. Longitudinal motion (z, through focus) is straightforward, yet lateral motion (xy) must be performed as a combination of rotation and translation. For this reason, measurements at arbitrary positions requires a rotated mask orientation (and incident illumination plane) dictated by the system geometry.

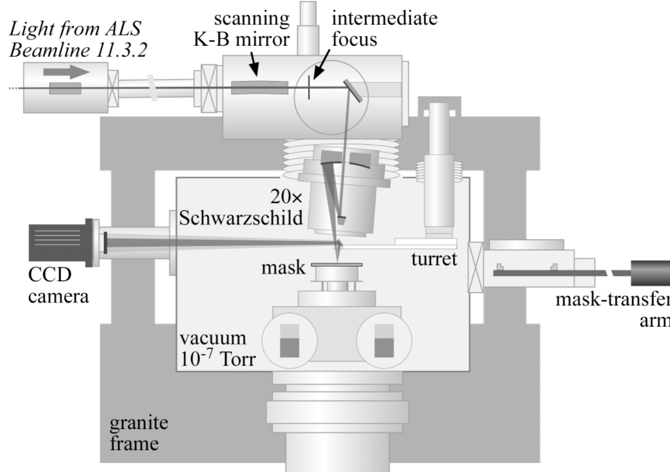

Fig. 1. The SEMATECH Berkeley Actinic Inspection Tool (AIT). Bending-magnet beamline 11.3.2 at the ALS provides tunable, monochromatic EUV light (λ = 13.4 nm) to the AIT. A K-B mirror pair brings the beam to an intermediate focal point above the main chamber. The horizontal element of the K-B scans laterally to increase the illumination area and uniformity. A 20× Schwarzschild objective serves as an illuminator, re-imaging the K-B focus to the mask with a divergence angle up to 0.0625 NA. Essential optical elements for the microscope rotate and translate on a 4-axis turret arm into the 2-cm gap between the mask and the Schwarzschild objective. The system operates at a base pressure of 6×10^{-7} Torr backfilled with oxygen to 6×10^{-5} Torr during operation.

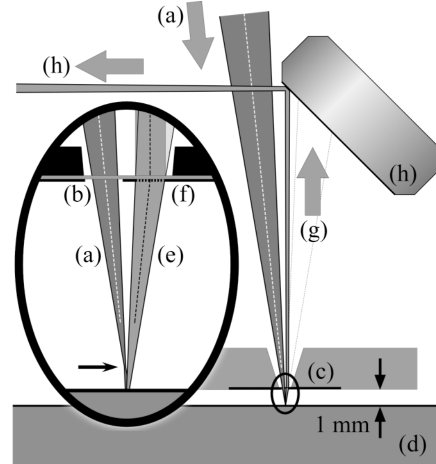

Fig. 2 In imaging mode, the incident, focused, 6° beam (a) passes through a window (b) in a patterned silicon nitride membrane (c) on its way to the mask (d). The mask is typically 100 to 300 μm below the illuminator's focal plane (black arrow) to increase the illuminated area. The reflected beam (e) meets an off-axis zoneplate lens with 0.0625 NA (f). The first diffracted order (g), bent vertically upward by the zoneplate, reflects from an ultra-flat multilayer-coated 45° turning mirror (h), sending the beam to the CCD camera. The off-axis design, allows the un-diffracted zeroth-order to miss the CCD without using an order-sorting aperture.

Table 1. Overview of AIT performance properties in the two modes of operation.

Mask-scanning mode

Bright-field Reflectivity testing
- → ≥ 1-μm spot
- → Reflectivity measurements to ± 0.1%

Dark-field Scattering
- → Finds defects not seen by non-actinic inspection tools.

Calibrated Reflectivity
- → Measuring the incident and reflected signals sequentially

Region-of-interest identification
- → Scans a larger area quickly.

Zoneplate Imaging Mode

Resolution (4× pixel over-sampling)
- → < 125 nm, mask
- → ~25 nm, 5× wafer equivalent
- → ~31 nm, 4× wafer equivalent

Exposure Time
- → ~0.5 s for alignment & navigation
- → ~10–20 s for highest resolution

Magnification
- → ~670×, direct to EUV CCD
- → 29.8-nm (mask) per CCD pixel

Illumination
- → 6° y-direction, with x-scanning
- → coherence: $\sigma < 0.2$

Field Size
- → 40 μm, based on CCD area and imaging magnification ratio

NA = 0.0625
- → emulates the solid angle of an 0.25-NA, 4× stepper

Through-focus
- → 0.05-μm z resolution
- → > 0.1-μm steps

Throughput
- → up to 450 images / 8-hour shift, 250–300 is typical

In *mask-scanning mode*, the mask moves continuously under the focused EUV beam, while the reflected light intensity is measured by a 1-mm-square photo-diode. Both bright-field (specular reflectivity) and dark-field (scattering) signals can be recorded.[3] In *imaging mode* (Fig. 2) a tiny Fresnel zoneplate lens projects an image of the illuminated mask surface onto an EUV CCD camera with a magnification of approximately 670×, or higher. The zoneplate's pupil is circular, and the numerical aperture (NA) is 0.0625, chosen to match the mask-side NA of an 0.25-NA, 4×, EUV stepper. Table 1 shows the typical operating parameters of the AIT, now running in routine operation.

3. PERFORMANCE UPGRADES

The AIT has undergone extensive upgrades to address initial fabrication and design limitations. The image details shown in Fig. 3 exemplify the progress that has been made. In 2005, vibration limited the resolution to several microns. System upgrades in 2006 focused on quenching vibration between the zoneplate and the mask, and on replacing the manual zoneplate alignment and control system with a four-axis computer-controlled stage. Following a re-design and complete overhaul of the optical imaging elements in early 2007, images such as Fig. 3(c) are now typical.

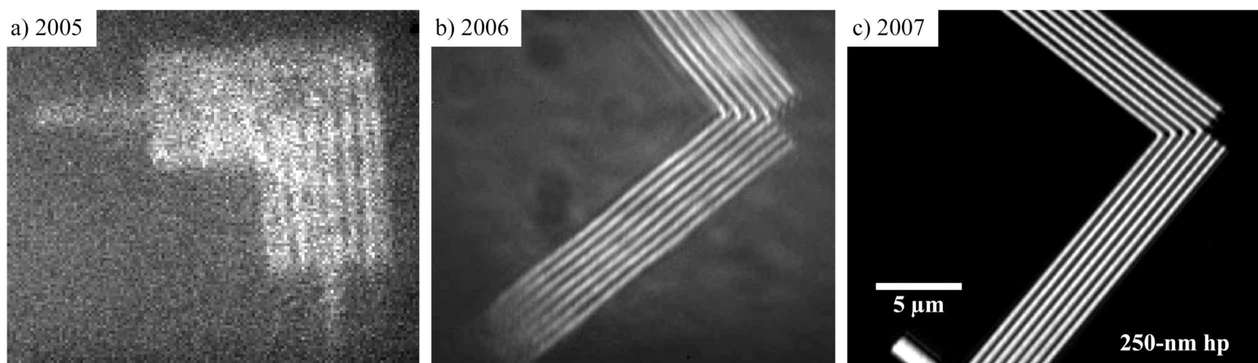

Fig. 3. AIT upgrades have delivered steadily improving performance since imaging mode first became operational in late 2005. Figures **3(a)** and **(b)** show details from examples of the best images recorded during 2005 and 2006 respectively; **3(c)** shows a typical image detail in scanning illumination mode. All images are shown on the same scale. *Mask image, courtesy of T. Liang, Intel Corp.*

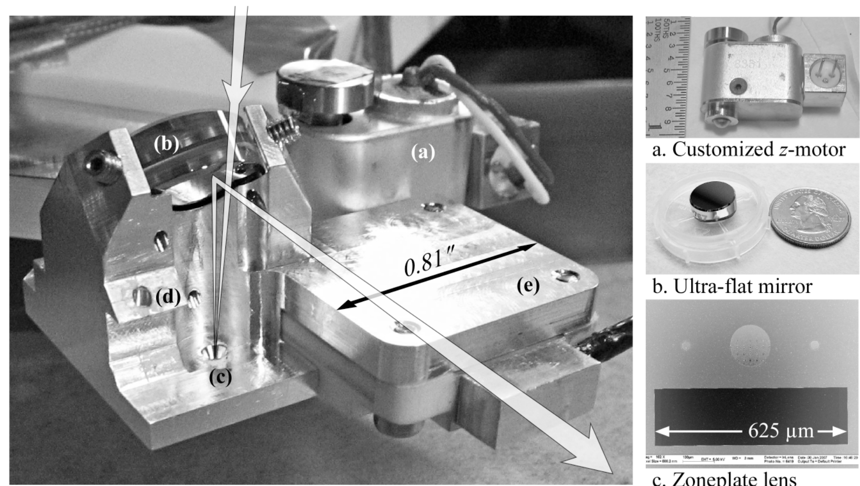

Fig. 4. Upgraded optical and mechanical components fit in a small vertical space (2 cm) between the reticle and the illumination Schwarzschild objective. (a) Customized Picomotor for through-focus actuation and image stabilization. (b) Ultra-flat, multilayer-coated, 45° turning mirror. (c) 0.0625-NA zoneplate lens with alignment features (held underneath). (d) Coarse beam alignment (angle and position) aid. (e) Capacitance gauge height sensor. The beam path, with two-reflections (mask, turning-mirror) is indicated by the white arrows.

The new optical elements for zoneplate imaging mode are described in Fig. 4. During measurement, this small optical system is suspended 1 mm above the mask surface, attached to a rotating and translating 'turret' arm. Elsewhere on the turret are the photo-diodes used in mask-scanning mode, and other components used for system and beam alignment.

To evaluate the imaging performance of the AIT, and the success of these upgrades, thousands of images were recorded during two separate measurement series. After the first series of measurements (July 2007), several subtle yet important

discoveries were made about the factors that degrade imaging performance, and ways we could overcome them. Among these factors were specific vibration sources (i.e. pumps), optical misalignment with respect to the zoneplate field of view, and the illumination conditions, including the mask height within the focused illuminating beam, and the controllable wavelength bandwidth. Once these and other issues were addressed, the performance of the AIT improved dramatically and a second set of benchmarking measurements was conducted (August/September 2007). Data from the second set are presented here. Figure 5 shows characteristic images from before and after the first round of benchmarking and upgrades.

In addition to the AIT hardware, countless software control system upgrades have been implemented to increase operational reliability and safety, improve system control and automation, and enhance data collection speed and record-keeping. These changes have yielded higher experiment throughput: now 250–350 images are routinely recorded in an 8-hour shift that includes mask loading.

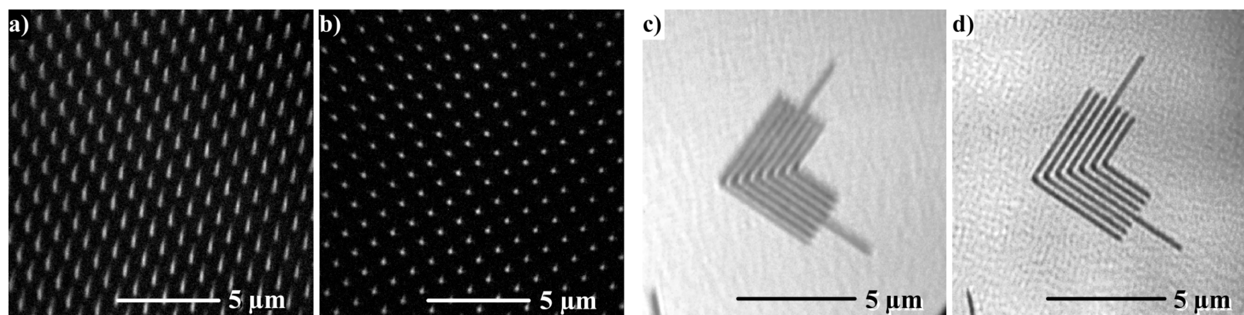

Fig. 5. Significant improvements in AIT imaging were based on learning from benchmarking testing conducted in July and again in late August, 2007. Shown are details of four AIT images from the same mask: before improvements, **(a)** and **(c)**, and after improvements, **(b)** and **(d)**. **(a)** and **(b)** are 175-nm (35-nm, 5× wafer equivalent) 1:5 contacts, revealing the improved point-spread function of the system. **(c)** and **(d)** is a 175-nm half-pitch (35-nm, 5× wafer equivalent) bright-field elbow pattern, showing much higher contrast in the second series of measurements.

4. ILLUMINATION

The imaging illumination conditions in the AIT are complex. Several steps have been taken to increase the illuminated area and the illumination uniformity and repeatability; several future upgrades are also being planned. Our measurements reveal a higher degree of coherence than initially anticipated for this tool, with σ close to 0.2.

The bending magnet beamline provides nearly coherent illumination across the entrance aperture (pupil) of the beamline. Therefore, the static beamline optical elements (K-B and Schwarzschild objective), which increase the illumination solid angle, do not reduce the degree of coherence. The coherence properties vary with operating conditions, including the longitudinal position of the mask. For example, in static illumination mode, with the mask in the Schwarzschild objective's focal plane, the illumination angles can be as high as 1.4 NA_o and 0.7 NA_o, in the x and y directions respectively, despite the high degree of coherence. When the mask is lowered by several hundred microns to increase the illumination area and uniformity, a given point on the mask surface sees a reduction in the effective illumination angles, and partial coherence σ values are expected to be below 0.2 and possibly below 0.1. Coherence estimation, based on the observed image contrast through focus is discussed in Section 7.

One major drawback of the static illumination is that reflectivity variations in the beamline optics (e.g. carbon contamination) can be projected onto the mask illumination pattern, degrading uniformity. While it is true that operating in the Schwarzschild's focal plane should eliminate many of these pupil non-uniformities, the illumination area in that plane is both narrow and sharply varying. As a compromise position, we operate the AIT with the mask 200–300 µm below the Schwarzschild's focal plane, where the illumination width is larger. This issue will be re-evaluated following illuminator upgrades in September 2007.

To eliminate chromatic aberrations, the imaging Fresnel zoneplate requires that the illumination bandwidth be limited to approximately $\Delta\lambda/\lambda < 1/1000$. The bandwidth is directly controlled by the monochromator exit slit width. We observe

that widening the exit slit (to increase the photon flux) produces a noticeable chromatic blur in the direction of the slit's opening (y-direction), perpendicular to the plane of the monochromator grating.

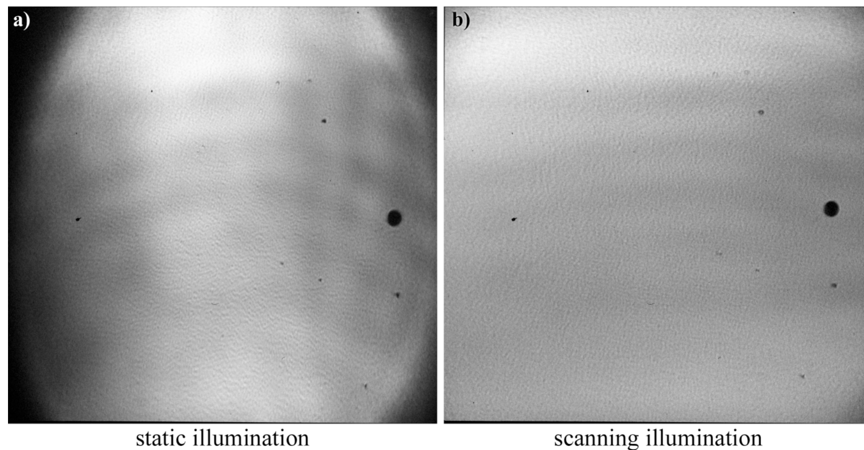

Fig. 6. Open field images recorded with **(a)** static illumination, and **(b)** (x-direction) scanning illumination. The full area of the CCD is shown, representing an area of the mask 40-µm wide. A mask region containing some noticeable defects (contamination) was intentionally selected to aid in finding focus. We believe that the small-scale structure arises from the mask and the coherent illumination, while large-scale structure comes from the illumination non-uniformity. The horizontal intensity bands may come from reflectivity variations (i.e. damage) in the beamline optics.

4.1 Scanning illumination

Adjusting the tilt of the beamline mirrors upstream of the Schwarzschild objective sweeps the illumination across the mask. Even small angle adjustments move the beam across the field of view. We have adapted these controls, coordinating their motions with the CCD exposures, to produce a more uniform illumination in the scanning direction (currently limited to the x-direction), as described in Fig. 6.

Controlled motion of the beamline optics during an exposure can be used to reduce the coherence[4]: here, a narrow, cone of coherent light moves across an angular range in time, yielding a partially coherent image. We note that when the system is operated with the mask below the focal plane of the Schwarzschild objective, the effective illumination angular range seen by a given point on the mask is reduced (the illumination sweeps past the point). Utilizing the coherence-reducing properties of temporally scanned illumination will require operating with in the mask in the Schwarzschild's focal plane.

4.2 Illumination uniformity

Illumination uniformity is a critical issue for aerial image analysis. It has been a central issue addressed in recent tool upgrades, and it continues to be a subject of ongoing work. Considering the image shown in Fig. 6(b), in the most uniform 8-µm-square patch (268 pixels wide) the measured illumination pattern varies by ±30% from its average value. It has been difficult to completely separate the illumination variation from local variations in the mask itself. Observations have shown that in all cases, the small-scale structures track the mask position exactly. Whereas, the slowly varying illumination changes remain largely stationary as the mask moves; thus they must come from the illumination. When the small-scale intensity variations are filtered mathematically, the remaining intensity variations can still be greater than 10% over the same 8-µm square region.

Mathematical post-processing of the images can achieve higher effective degrees of uniformity by providing accurate, flexible image intensity normalization. Normalization performed without a so-called "flat-field" image to use as a reference, requires the detection of slowly varying intensity changes that occupy a separate length scale range from the image features of interest. Such processing is most straightforward within a large-scale pattern of repeating features, yet it is very difficult for arbitrary or isolated patterns. For this reason specifically, experimental mask patterns can be designed to improve the actinic inspection quality. This should be considered in future experiments.

4.3 Illumination repeatability

Illumination repeatability is a separate issue from uniformity, describing the extent to which consecutive images will produce the same result. A complete assessment of the AIT's imaging reliability has not yet been performed, but some consistent observations have been made.

In static illumination mode, consecutive measurements produce results that appear indistinguishable. However, when the mask moves, the illumination changes in subtle ways. Intentional lateral motion of the mask during navigation can cause micron-scale displacements of the zoneplate which, due to the high imaging magnification (> 680), lead to apparent shifts in the illumination. Furthermore, moving the mask through focus also changes the illumination. The off-axis, non-telecentric imaging, combined with the divergent, Schwarzschild illumination causes the mask to move through the stable pattern of the illumination's non-uniformities. Provided that the optics can be cleaned and improved, these effects are expected to improve over time.

Some imaging systems are designed to record flat-field images for normalization based on the measured intensity pattern. This method beaks down when the illumination pattern is structured in any way and moves unpredictably.

5. FLARE

In lithography, *flare* arises when light from bright regions of the mask scatters into the surrounding areas in the projected image. Flare reduces image contrast by casting light into regions intended to be dark. It can be especially acute for small dark features in bright regions, and the relative flare magnitude typically increases with shrinking feature size.

Aerial image flare has been a concern since the inception of the AIT[5] owing to its use of a diffractive Fresnel-zoneplate lens as the image projecting element. The scattering and flare magnitudes of zoneplate lenses, which for EUV wavelengths are typically fabricated by e-beam lithography, are largely unknown, and must be highly case specific and therefore difficult to generalize. For these reasons specific tests to measure flare in the AIT are particularly interesting.

A short-range flare measurement was performed by recording the illumination intensities at the central vertex of several dark crosses in a large bright region. Using photo-resist to measure intensity levels, this technique has been used successfully to evaluate flare in EUV lithography tools[6]. The cross line-widths studied were 0.5, 1.0, 2.5, and 5.0 µm on the mask (100, 200, 500, and 1000 nm, 5× wafer equivalent dimensions). The total area of the mask illuminated in these tests was limited to the width of the AIT's field of view, approximately 40 µm. For each measurement an image of the cross was recorded and then normalized to an image of an open bright region 100 µm microns away, recorded immediately afterward as a 'flat field' normalization. To remove the additive effects of dark current in the CCD camera, for each set of images the CCD's background-level was carefully measured. These background readings, subtracted from each image, are based on a series of three consecutive images recorded with no light in the chamber and exposure times identical to the subject data. (Note: this background subtraction method was followed for all of the imaging data presented in this report.) Finally, images were recorded of the dark, absorber region to measure the baseline intensity level in dark areas. The values extracted from these absorber images were selected from the same pixel locations within the CCD image as the cross vertex locations.

Flare measurement in the AIT is complicated by the absence of a synchronized shutter (an upgrade is planned). Without a shutter, light continues to fall on the CCD during image readout (in static illumination mode only). Exposure times for these measurements were 17 seconds (a typical value), and the high-resolution readout time is 1.7 seconds. We observe that in static illumination mode, the intensity levels in dark regions is higher than in scanning mode. With static illumination, the pattern of light intensity on the mask image is a centered, vertical stripe. Image pixels from the lower portion of the image receive the highest additional signal level because they pass through the entire length of the illuminating stripe before being read out. In scanning mode, the illumination light intensity sweeps across the field of view, and is steered off the CCD camera before readout. Hence, in this mode, the absence of a shutter and the finite readout time do not affect the measurement.

Figure 7 shows details of four scanning-mode cross images from which flare measurements were made. The measured flare values and baseline absorber reflectivity levels are shown in Fig 8. The error bars indicate the minimum and maximum relative intensity values observed within a small region near the cross center; the connected data points were recorded at the geometric centers. The absorber region intensity levels, calculated at the same positions in the camera image as the four cross positions, were $3.06 \pm 0.28\%$ for static illumination, and $1.30 \pm 0.04\%$ for scanning illumination.

The data reveal flare magnitudes of approximately 2–3% above the absorber background level, depending on feature size. At the 0.5 µm line size, lens aberrations may have affected the measured flare value. In static illumination mode, the absence of a synchronized shutter reduces contrast in bright-field images, nearly doubling the apparent flare magni-

tude. This data is consistent with other observed contrast differences between static mode and scanning mode measurements of the same patterns. We expect that the apparent flare levels in the two modes will match the scanning illumination mode data once a shutter has been installed.

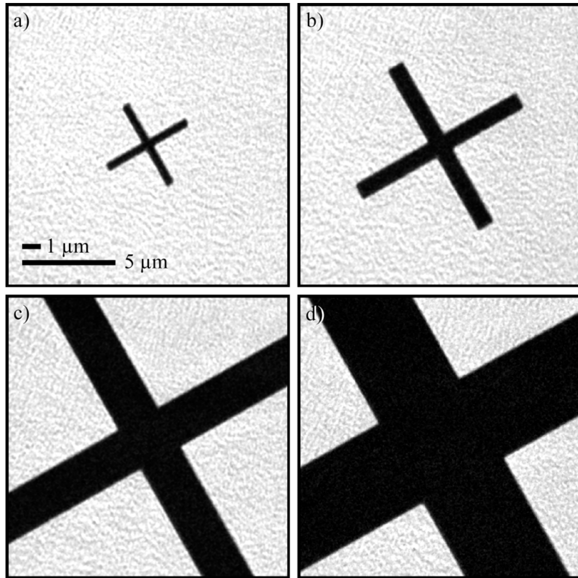

Fig. 7. Details of four scanning-mode cross images from which flare measurements were made. On the mask, the line widths are **(a–d)** 0.5, 1.0, 2.5, and 5.0 µm, respectively.

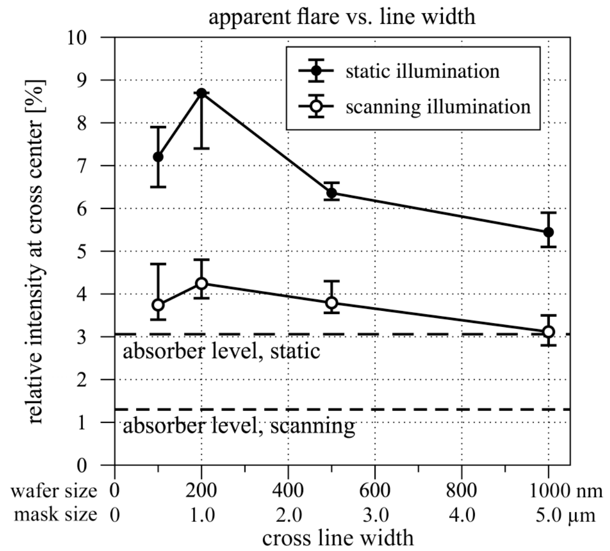

Fig. 8. Measured relative intensity at the centers of four dark cross patterns in a large bright field, recorded with both static and scanning illumination.

6. MODULATION TRANSFER FUNCTION—MTF

The MTF of an optical system is the ratio of the modulation in the image to that in the object as a function of the feature size. The MTF of a high-quality imaging system is a function of its illumination coherence properties, the pupil's shape and numerical aperture, and the incident light wavelength. Coherently illuminated systems are expected to maintain high contrast, with a sharp drop near the resolution limit. Partially coherent optical systems typically have a range of illumination angles that causes the contrast to roll off more gradually for smaller feature sizes. Aberrations, can reduce the contrast, and hence the MTF: their contributions may vary with both the direction and size of features being imaged.

For the MTF measurements, elbow patterns with (mask) critical dimension (CD) sizes from 100 to 500 nm and two different rotational orientations were evaluated for their contrast behavior through focus. Both bright-field (BF) and dark-field (DF) patterns were imaged. The presence of astigmatism required the collection of a broad enough focal range to include the best focus in each of the four directions, 0°, 90°, 45°, and 135°. This measurement involved the extraction of elbow pattern regions from each image, intensity normalization across the line region, and the systematic evaluation of the contrast for the central three elbow lines, averaged over several pixels along the length of the line. Figure 9 shows several representative elbow pattern images close to best focus. Data from these complete measurements appears in Fig. 10. Note that the object (mask) modulation was considered to be slightly less than 100% (97.4%), based on the measured light intensity in the pure absorber regions (as discussed in Section 5).

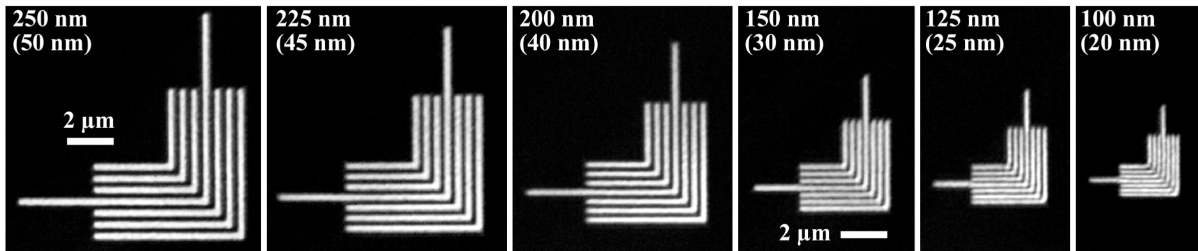

Fig. 9. Representative 0°-90° elbow patterns used in the calculation of the dark-field MTF. A finite astigmatism magnitude makes the contrast higher in one direction or the other, through focus. These images are close to *best focus* in each case. All images are shown on the same size scale.

The data show slightly lower contrast values for the bright-field patterns. The magnitude of this difference (typically several percent) is consistent with the contrast-loss mechanisms discussed in Section 5: primarily flare, and the absence of a light shutter. Not addressed in this study are the limits of the test mask's quality. Although dark-field elbows were clearly resolved as small as 100-nm CD, bright-field features below 125-nm were not usable.

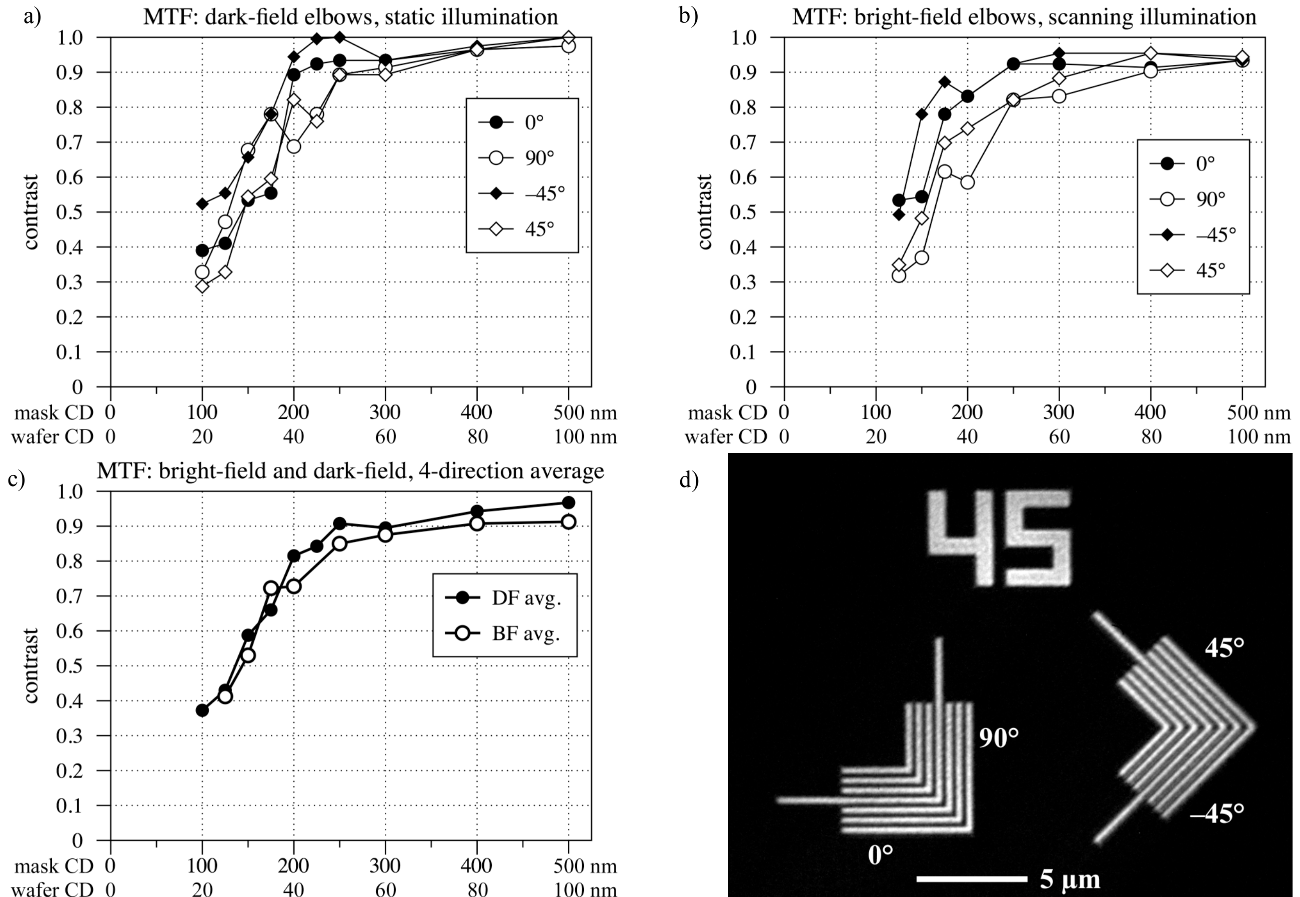

Fig. 10. Calculation of the MTF was performed by evaluating contrast in both bright and dark field elbow patterns in four line orientations. **(d)** A detail of a typical image from a through-focus series, close to focus; the "45" label indicates a 5×, wafer equivalent size. The angle definitions assigned to the four branches are shown. **(a)** MTF calculated for dark-field elbows in all four line-directions. **(b)** A similar calculation for bright-field scanning illumination. **(c)** The average contrast values in the two series are compared.

7. COHERENCE MEASUREMENT

Additional information about the degree of coherence can be extracted from the contrast through focus, when the measurement range is large enough to include the first *lobes* of the contrast function and a range of feature sizes are included. Data for several feature sizes has been collected and will be published subsequently. Figure 11 shows two such measurements extracted from 150-nm (30-nm, 5× wafer equivalent) bright-field elbow patterns under static illumination.

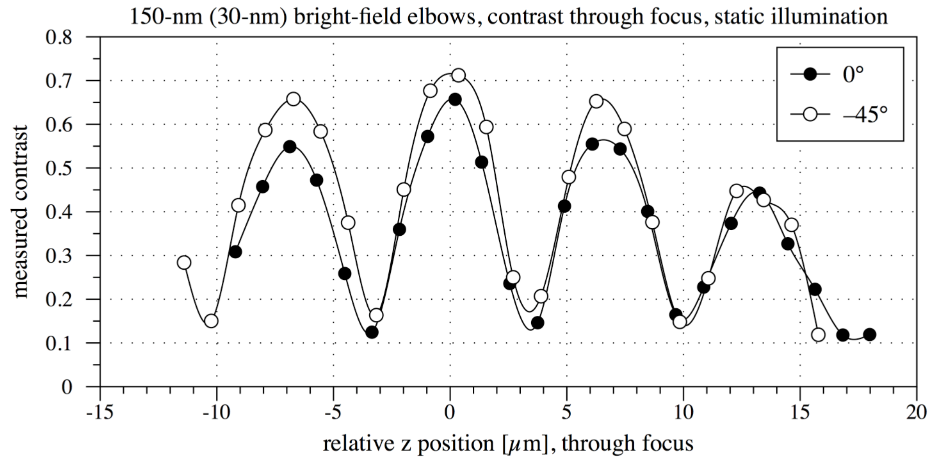

Fig. 11. Measured contrast in a large through focus series: bright-field 150-nm elbows (30-nm, 5× wafer equivalent) in the 0° and –45° orientations. Static illumination. Above and below the plane of best focus, the high image contrast returns. This behavior indicates a low σ value.

Similar measurements of 125-nm, 175-nm, 200-nm, and 250-nm patterns show first-lobe contrast values near 90% of the contrast at best focus; this behavior is consistent with a σ value of 0.2, or lower.[7]

8. ABERRATIONS

Aberration measurements have revealed that astigmatism is currently the dominant aberration affecting the imaging performance of the AIT. Astigmatism causes the plane of best focus to shift longitudinally for pattern features oriented in different directions. Astigmatism can arise if the zoneplate lens is tilted from its optimal plane, if the central ray is not aligned with the center of the field of view of the lens, or if there were an asymmetry in the fabrication of the zoneplate. The alignment issue is important because it may be possible, by adjusting the illumination angles, to find a position of minimum astigmatism within the field. Such investigations are currently in progress. Alignment freedom is constrained by the fixed angle of the turning mirror, which is currently not adjustable in situ.

Elbow patterns are often used as a resolution target because they reveal the presence of astigmatism in a through-focus series, as shown in Fig. 12. With astigmatism, lines oriented in different directions will achieve their highest contrast values in different planes. Figure 13 contains an analysis of the *astigmatic displacement*, the longitudinal separation between the best focus planes for the two pairs of orthogonal line directions. These measurements were extracted from the same data used in the dark-field MTF calculations. While a given astigmatism magnitude carries a greater significance for smaller CD values, the astigmatic displacement should not vary unless there are other aberrations present in the lens.

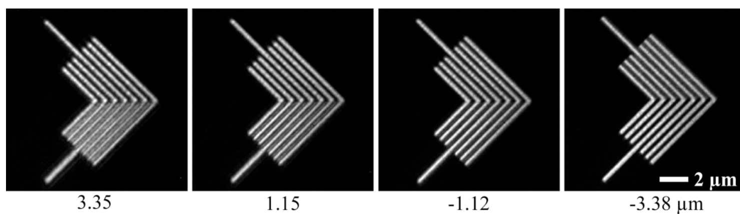

Fig. 12 (above). 45° astigmatism is visible in this series of images of 250nm (50-nm) dark-field elbows. The same contrast analysis through focus used in the MTF calculations is here used to identify the best focus planes for the two directions. The relative *z* position of each image is shown in μm.

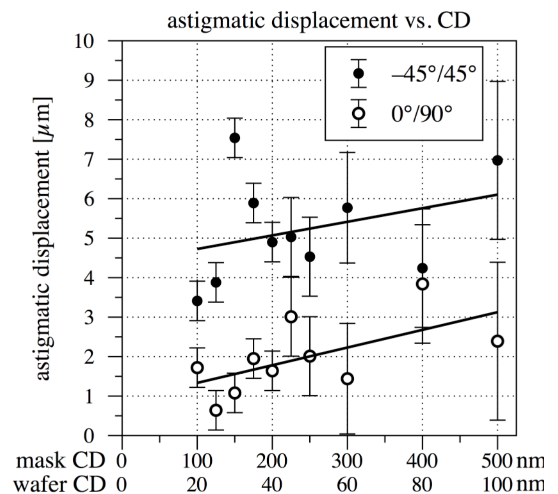

Fig. 13 (right). The contrast measurements used to extract the dark-field MTF were used to determine the astigmatic displacement for each available CD value, in both elbow directions. The error bars here indicate the through-focus step size used in the measurements.

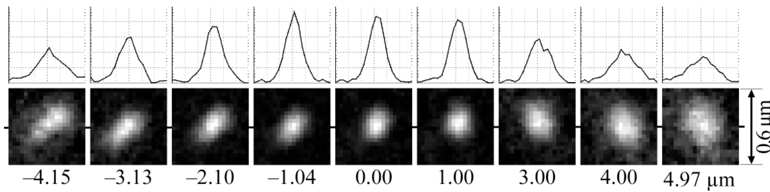

Fig. 14. Images of one 175-nm (35-nm) contact, followed through focus, reveal a sharp point-spread function, yet several microns of astigmatic displacement. Each image and profile are 600-nm wide. Relative focus displacements are given below each image, in μm. The images are centered on the points of maximum intensity, and horizontal line profiles through those points are shown.

A different method for assessing aberration magnitudes involves observing the imaging behavior of point-like patterns, such as contacts, through focus. Figure 14 shows an example of a single, arbitrarily selected, dark-field, 175-nm contact (35-nm, 5× wafer equivalent) followed through focus. The astigmatic behavior is revealed in the way the elliptical shape changes orientation by 90° on either side of focus.

The analysis of coma and spherical aberration are the subjects of ongoing research. If present at sufficient magnitude, coma would asymmetrically distort the elbow pattern in one orientation more than others. Spherical aberration may be detectable through a change in the image line widths observed through focus. Neither effect has been studied in sufficient detail to reach conclusions aside from the observation that these aberrations, if present, must be relatively small.

9. LINE EDGE ROUGHNESS

Line-edge roughness (LER) and line-width roughness (LWR) are two important metrics used to evaluate both photoresist and reticles. Measuring LER and LWR accurately, in any tool, requires highly uniform illumination over the evaluation area, and an understanding of the illumination coherence properties. Non-uniformity and coherence can change the appearance of the lines and the LER/LWR measurements making accurate evaluation difficult.

The AIT's ability to record a detailed view of the aerial image makes it a powerful tool for understanding the effects that contribute to LER, independent of the properties of photo-resists and resist-processing. This is true provided that the illumination is sufficiently uniform and the coherence properties are known. Since the AIT images are recorded digitally, careful image intensity normalization can be performed, so long as the processing does not degrade the data on the length scales of interest to LER/LWR measurement.

We find in the AIT that aerial image measurements of line patterns at best focus show static, repeatable, granular variations (typically 5–20% relative intensity changes) in the bright regions. These variations are always present, yet differ in magnitude from mask to mask; their nature and origin are now under investigation. These small-scale variations are stable over time and follow the mask pattern exactly. If the variations we observe are due to small phase changes in the reflected light field, then we predict that their appearance, like speckle, will be dependent on the illumination coherence properties, and the (mask dependent) magnitude of the phase variations[8]. Whatever their specific origin, their presence affects the apparent LER/LWR measurements by introducing small-scale intensity variations at the line edges.

As a first step in the evaluation of the LER/LWR performance of the AIT, one-dimensional dense-line images were recorded through focus. The image intensities were normalized using a smooth Fourier-domain filter that preserved only the lowest spatial frequencies. The images recorded closest to best focus were selected based on the minimum LER value. Within those images, an 8-μm long region was used for evaluation. Measurements from 18 individual lines in each image, and for two CD values, are compiled in Table 2.

Table 2. LER and LWR 3σ values for dense lines with two CD sizes. The sizes are given in mask units; the parentheses contain the equivalent sizes on the wafer with 5× demagnification.

CD (wafer) [nm]	LWR [nm]	LER [nm]
250 (50)	21.82 ± 2.64 (4.36 ± 0.53)	16.10 ± 2.19 (3.22 ± 0.44)
220 (44)	18.61 ± 1.97 (3.72 ± 0.39)	13.79 ± 1.57 (2.76 ± 0.31)

These measurements will be repeated as future, planned upgrades to the AIT illumination system are performed. One interesting experiment to perform would measure the mask with series of small displacements in order to determine what fraction of the measured LER/LWR comes from noise and what fraction is a repeatable (albeit coherence dependent) property of the mask.

10. FOCAL PLANE TILT

A number of tests have revealed a significant focal-plane tilt of several microns across the field, oriented primarily in the *y*-direction (vertically across the CCD camera image). The possibility of field-dependent astigmatism variation complicates this measurement somewhat when elbow patterns are used as an indicator of focus. To remove this ambiguity, a focus assessment was performed using a field of contacts, measured through-focus. The calculated focal plane or *surface* includes tilts that may arise from misalignment of the zoneplate, combined with tilt and non-flatness of the mask plane itself, which cannot be separated within this measurement.

In the presence of a small amount of astigmatism, the shape of the observed contact images changes through focus (becoming elliptical). This effect was used to identify the best-focus plane for numerous *xy* positions in the field of view of the CCD. Figure 15 shows an image of the contact field used in this study, and a contour plot of the best focus positions within the set of measurement points where good data was available.

The data show that focus changes by approximately 7 μm vertically across the image. This value is surprisingly high considering that it suggests a slope of over 10 degrees. This amount of tilt, is a mechanical impossibility for the zoneplate alone. Although the contour plot in Fig. 15 reveals a surface that is not a perfect plane, a plane fit to the available data shows an *x*-direction tilt of –2.29°, and a *y*-direction tilt of –13.3°. It will be worthwhile to conduct this test in different ways and investigate other sources of the large focal plane tilt, such as a large misalignment out of the zoneplate's intended field of view.

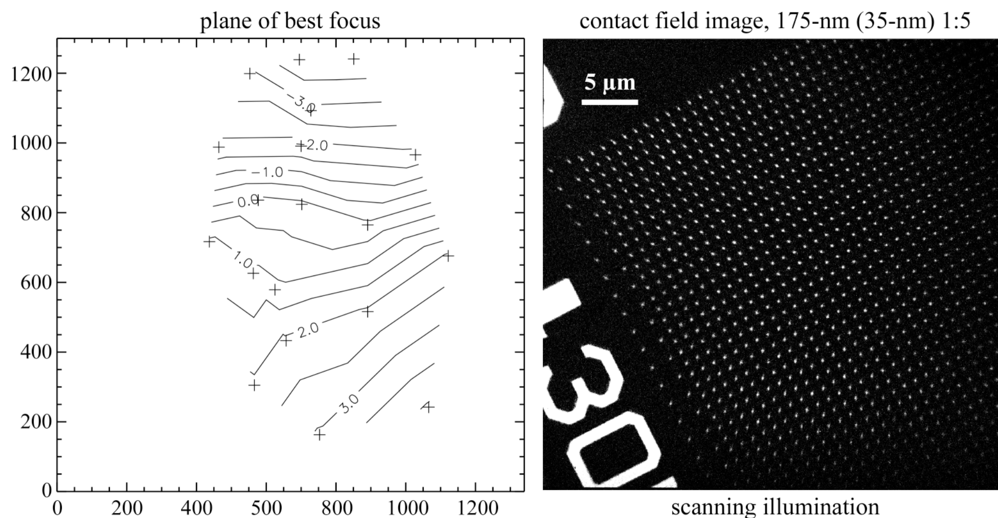

Fig. 15. The shape of the focal plane was measured by assessing images of a field of small contacts, recorded through focus. The image shows an array of 175-nm (35-nm wafer equivalent size), 1:5 contacts. Measurement positions are indicated in the contour plot by "+" symbols. The contour labels show longitudinal displacement in microns from an arbitrary plane. The axes labels show the camera position, in pixels.

11. CONCLUSION

The AIT is a unique and highly productive instrument serving the EUVL research community with routine operations. The performance of the AIT has improved dramatically over the past few months and will continue to advance with the completion of several planned upgrades. During initial operation in 2004 and 2005, when the AIT's imaging performance was well below specification, large scale upgrades were required to achieve progress. Now that the imaging performance has improved, further optimization requires careful experiments, detailed analysis, and clever, judicious future upgrades.

The MTF measurements show high contrast imaging down to 200-nm mask-CD size (40-nm, 5× wafer equivalent). Below that level, good contrast is maintained yet with a steady roll-off toward 100-nm (20-nm) where it reaches 30–50%, depending on line orientation. Measurements of smaller CD values were not performed.

Flare had been a major concern and significant unknown for zoneplate imaging. Our recent investigation to measure flare directly has shown that with scanning illumination, the zoneplate flare level is on the order of 2–3%, factoring in the 1.3% absorber reflectivity. We have also confirmed that the absence of a synchronized shutter introduces an addi-

tional 2–4% effective flare magnitude that depends on the exposure time, the surrounding pattern, and the image position within the CCD camera's field of view.

The illumination coherence of the AIT is much higher than a conventional lithographic stepper, and that fact must be taken into consideration when modeling the imaging performance of the tool. We observe strong, small-scale intensity variations in bright areas that may impact the measured LER/LWR and must be investigated further. Specific tests the measure the LER and LWR from dense line patterns reveal LWR 3σ values on the order of 20 nm (4 nm, 5× wafer equivalent), and LER 3σ values close to 15 nm (3 nm, 5× wafer equivalent) for the specific mask measured here.

Aberrations in the imaging performance are dominated by astigmatism and a tilted focal plane. Their interaction complicates precise assessment with the available data. The astigmatic displacement may be as high as 5–6 µm, which suggests approximately 2–2.5 nm of RMS astigmatism. Through continued measurement and re-alignment, it may be possible to reduce or overcome the astigmatism in the near future.

Only by conducting experiments such as these, testing the imaging performance limits, can the AIT continue to improve. Experience has shown that so-called *benchmarking* work is time well spent—it leads directly to higher-quality measurements and increased tool throughput. Continuing to upgrade the AIT takes time, and will require careful planning not to disrupt its productivity.

ACKNOWLEDGMENTS

The authors gratefully acknowledge Obert Wood II of AMD, the former SEMATECH project manager who guided and supported this project from inception through 2006. Yanwei Liu played a key role in the early development of the actinic inspection tool. Valeriy Yashchuk of LBNL performed optical testing of several ultra-flat turning mirror samples. John Taylor of LLNL provided many helpful insights. This work was performed under the auspices of the U.S. Department of Energy by University of California Lawrence Berkeley National Laboratory, and Lawrence Livermore National Laboratory, and is funded by SEMATECH under Project LITH-343.

REFERENCES

1. A. Barty, Y. Liu, E. Gullikson, J. S. Taylor, and O. Wood, "Actinic inspection of multilayer defects on EUV masks," *SPIE* **5751**, 651–659 (2005).
2. Y. Liu, A. Barty, E. Gullikson, J. S. Taylor, J. A. Liddle, O. Wood, "A dual-mode actinic EUV mask inspection tool," *SPIE* **5751**, 660–669 (2005).
3. K. A. Goldberg, A. Barty, P. Seidel, K. Edinger, R. Fettig, P. Kearney, H. Han, O. R. Wood II , "EUV and non-EUV inspection of reticle defect repair sites," *SPIE* **6517,** 65170C-1-7 (2007).
4. P. Naulleau, K. Goldberg, P. Batson, J. Bokor, P. Denham, and S. Rekawa, "A Fourier-synthesis custom-coherence illuminator for EUV microfield lithography," *Appl. Opt.* **42** (5), 820–26 (2003).
5. A. Barty, H. Chapman, D. Sweeney, R. Levesque, and J. Ayers, "Actinic Mask Inspection at the ALS: Initial Design Revew," *VNL EUV Mask Blank Technology Transfer Program*, April 3, 2003,UCRL-CR-152460.
6. J. P. Cain, P. Naulleau, C. J. Spanos, "Lithographic measurement of EUV flare in the 0.3-NA micro exposure tool optic at the Advanced Laser Source," *SPIE* **5751,** 301–311 (2005).
7. P. P. Naulleau, *personal communication.*
8. P. P. Naulleau, "Relevance of mask-roughness-induced printed line-edge roughness in recent and future extreme-ultraviolet lithography tests," *Appl. Opt.* **43** (20), 4025–32 (2004).